Strain and filler ratio transitions from chains network to filler network damage in EPDM during single and cyclic loadings

Nicolas Candau, Oguzhan Oguz, Edith Peuvrel-Disdier, Jean-Luc Bouvard, Christophe Pradille, Noëlle Billon

Strain and Filler Ratio Transitions from Chains Network to Filler Network Damage in EPDM during Single and Cyclic Loadings

Nicolas Candau [1,*,a], Oguzhan Oguz [2], Edith Peuvrel-Disdier [1], Jean-Luc Bouvard [1],

Christophe Pradille [3], Noelle Billon [1]

[1] Mines ParisTech, PSL Research University, CEMEF - Centre de Mise en Forme des Matériaux, UMR CNRS 7635, CS 10207, 06904 Sophia-Antipolis, France

[2] Laboratory of Macromolecular and Organic Materials (LMOM), Institute of Materials (IMX), Ecole Polytechnique Fédérale de Lausanne (EPFL), Station 12, 1015 Lausanne, Switzerland

[3] Mat-xper, 06560 Valbonne, France

[*]Corresponding author: nico.candau@gmail.com

[a] Presently at: Centre Català del Plàstic (CCP), Universitat Politècnica de Catalunya, C/ Colom, 114, 08222 Terrassa, Spain

Abstract

Chains and filler network damage were investigated during single and multiple cycles on a series of vulcanized EPDM containing various filler contents. In both series of experiments, a strain and a filler ratio transitions for damage mechanisms were identified. For low filler content (≤40 phr), damage mechanisms mostly occur in the elastically active rubber network consistent with the chains network alteration theory associated with irreversible chains scission/bond breakage. For high filler content (>40 phr), a strain transition occurs with damage initially located in the elastically active rubber network, but subsequently localizes in the vicinity of the filler-filler network. This is ascribed to filler re-aggregation with strain, improving its load-bearing capacity, that may release the immobilized rubber formed by the chains that are occluded and bonded to fillers. During cyclic experiments, such reversible release involving loss of weak physical bonds and chains slippage yields in a progressive cavity closing with cyclic accumulation that prevents further irreversible damage of the elastically active rubber network.

Introduction

The resistance of filled elastomers to mechanical solicitations is governed by its capacity to control the nucleation, growth and coalescence of voids favoring crack growth path and yielding to their macroscopic failure. Understanding the relationship between this macroscopic damage and its associated molecular mechanisms is of major importance to improve the rubber mechanical performance in industrial applications.

One example of such industrial applications is the mechanical devulcanization, i.e. the breakage of chemical crosslinks by loading, one promising rubber recycling route [1]. Mechanical devulcanization is of special interest for EPDM, a synthetic rubber usually difficult to recycle via conventional chemical devulcanization techniques [2]. Hence, the devulcanization process of

such materials still requires in-depth investigations. Its efficiency depends on the loading conditions such as the number of cycles, the cycling rates, and the maximum applied load [3]. Such loading conditions applied to filled rubbers reveal a softening mechanism, so-called Mullins effect [4], whose molecular mechanisms at its origin are still under debate in the literature.

Given their complex nature, amorphous or semi-crystalline elastomers like EPDM may exhibit viscoelasticity, viscoplasticity, strain-induced crystallization and damage. Digital Image Correlation (DIC) is a convenient mean to isolate damage to other large strain mechanisms in cyclic loading (Mullins damage) and in single loading. Like dilatometry [5], such technique provides access to the volumetric strain, associated with voids fraction [6]. Recent advances permitted to reach high spatial resolution by SEM-DIC [7] and re-build of volume via Digital Volume Correlation [8]. DIC has been used to evidence a delay in voids opening/closing in Mullins' type loading in comparison to single loading [9]. However, DIC has not been exploited yet to identify such damages at the molecular scale. Other techniques might be employed to give insight on strain-induced damage in rubbers at nano/microscale, such as X-Rays Micro-Computed Tomography (μCT) [10], X-Rays scattering (SAXS) [11] or light scattering (SALS) [12]. Creton et al. demonstrated the creation of new nanovoids with incremental strain rather than to the reopening of previously created cavities as probed by real-time SAXS experiments during cyclic loading [11]. While showing mechanisms at more local scales, as compared to DIC, these radiation techniques still do not provide direct information on rubber damage at chains network scale.

To address this question, real-time experiments have recently been developed. By combining Electron Spin Resonance (ESR) and stress–strain data, Suzuki et al. [13] highlighted the

contribution of chain scissions to the Mullins softening in Silica filled SBR. Clough et al. exploited strain-induced light emission from mechanoluminescent cross-linkers in silica-filled poly(dimethylsiloxane) to demonstrate the participation of covalent bond scission to the Mullins effect [14]. While these real-time techniques require *ad-hoc* materials with appropriate surface treatment of particles [13] or modified crosslinkers [14], they give interesting perspective on the contribution of molecular damage associated with deformation mechanisms in industrial rubber systems. There is however still few experimental studies performed on industrial or model rubbers to confirm the multiple molecular mechanisms occurring during single loading tests or cyclic tests associated with the Mullins effect, like those proposed in physically-based modelling such as bonds rupture [15], molecules slipping at the matrix−filler interface [16], rupture of clusters of fillers [17] or disentanglements [18].

We have recently developed an experimental method for the real-time identification of strain-induced chains network damage in EPDM [19], [20]. In the present study, this method is applied to EPDM with various filler contents subjected to multiple cycles. The aim is to identify damage mechanisms under deformation conditions close to that of mechanical devulcanization, which is of significance for industrial rubber recycling applications. First, damage mechanisms were investigated during single loading up to failure and during loading-unloading. Secondly, we investigated the Mullins effect by applying cyclic loadings with incremental strain. In all series of experiments, strain and filler ratio transitions in damage mechanisms were identified, suggesting (i) damage to be predominantly localized in the rubber chains network in weakly filled EPDM ($\varphi \leq 40$ phr) and (ii) a strain transition from rubber chains network damage to filler network damage to occur in highly filled EPDM ($\varphi > 40$ phr).

2. Materials and methods

2.1. Materials composition and processing

The materials provided by the SACRED Group are extended oil carbon black filled EPDM (Keltan 5470) obtained by sulphur vulcanization of the gum. They contain 70% in mass of Ethylene and 4.6% of ethylidene norbornene (ENB). All materials contain 80 phr (80g per 100 g of rubber) of carbon black (N550), 4 phr of calcium oxide, 5 phr of zinc oxide, 1 phr of stearin, 2 phr of Polyethylene Glycol (PEG 4000) as plasticizer. The vulcanization components are 1.2phr of sulfur (75%), 1 phr of mercaptobenzothiazole (MBT 75%), 0.8% phr of mercaptobenzothiazole disulfide (MBTS 75%), 1.2 phr of N-cyclohexyl-2-benzothiazolesulfenamide (CBS 75%) and 1.5 phr of zinc dialkyl dithiophosphate (ZDTP 70%). An internal mixer (Brabender®) is used for the rubber compounding. Sample sheets are produced by curing in a hot press at 170°C for with a curing time $t_{100\%}$ =15 minutes, a time corresponding to the moment when the torque reaches 100% of maximum RPA. Dumbbell-shaped samples, with a 15 mm gauge length (L_0), 6 mm thickness and 10 mm width, are then prepared for tensile testing.

2.2. Digital image correlation (DIC)

An electromechanical tensile test machine (INSTRON 5960) is used to perform mechanical tests (both loading and unloading) at room temperature. The nominal tensile strain rate of $1s^{-1}$ is applied for these tests. A four-cameras setup consisting of two-pairs systems is used to record the displacement fields on both front and side faces of the sample (Figure 1a). The post-processing of a series of images recorded is performed using VIC-3D software package. 3D DIC displacement data are converted into strain values (Figure 1b,c). λ_1 represents the stretching ratio in the tensile direction, whereas λ_2 and λ_3 correspond to the transversal stretching ratios in the

directions of the sample width and thickness, respectively. As described in our previous work [21], the transversal and longitudinal strains are homogeneous in the center of the sample and significantly decrease close to the clamping zones. The strain fields in both front and side surfaces are determined from a region of interest (ROI) in the central part of the sample. Details on the choice of DIC parameters can be found in ref [21]. The true stress is defined as the ratio between the applied force F and the specimen cross-section:

$$\sigma_T = \frac{F}{L_0 e_0 \lambda_2 \lambda_3} \tag{1}$$

where L_0 is the initial length and e_0 the initial width. The volumetric strain $\Delta V/V_0$ is defined as:

$$\Delta V/V_0 = \lambda_1 \lambda_2 \lambda_3 - 1 \tag{2}$$

The anisotropy factor associated with volumetric strain is defined as follows:

$$A = \left| \frac{\varepsilon_1}{\varepsilon_2 + \varepsilon_3} \right| \tag{3}$$

where $\varepsilon_i = \lambda_i - 1$ (i=1;2 or 3). Rubber samples are stretched at different maximum strains. As seen in Figure 1c, the transverse and longitudinal strains are homogeneous in the center of the sample and significantly decrease close to the clamping zones. The strain field in both front and side faces are obtained in the central part of the sample. Table 1 details the maximum displacement (in mm) reached for all loading-unloading tests for the series of materials. Various maximum local strains reached during the loading phase and calculated by Digital Image Correlation are provided in table 1. After performing the tensile tests, the specimens are stored at room temperature prior to ex situ swelling and thermoporosimetry experiments.

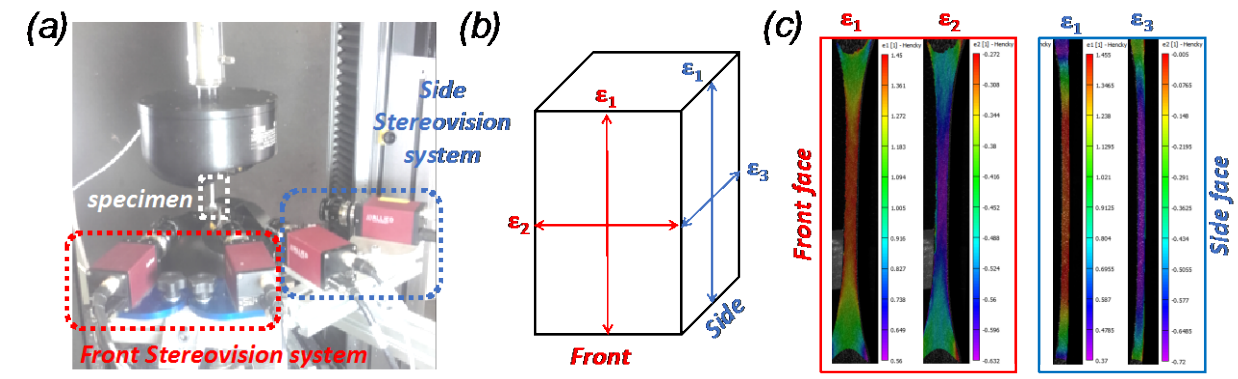

Figure 1. *(a)* Experimental Digital Image Correlation (DIC) set-up based on two independent stereo-vision systems to measure simultaneously strain fields on front and side surfaces of specimen, *(b)* Schematic representation of the front and side faces of the specimen with directions of the principal strain ε_1 on front and side face, ε_2 on front face and ε_3 on side face. ε_1 is calculated as the average value obtained on front and side surfaces, *(c)* longitudinal and transverse strain fields analysed on front and side faces of the specimen for a given macroscopic deformation.

	Maximum displacement reached during loading (mm)				
	0	30	60	90	120
Sample code	Maximum longitudinal strain λ_1 reached during loading (mm)				
F0	1	X*	3.38	4.25	4.9
F20	1	2.08	2.92	3.72	4.13
F40	1	2.03	2.84	3.66	4.34
F60	1	1.98	2.67	3.46	4.36
F80	1	1.88	2.77	3.64	3.86 **

Table 1. Maximum displacements (in mm) and associated longitudinal strain λ_1 reached during loading phase of the loading-unloading tests for the series of materials F0, F20, F40, F60 and F80.

* Test was not performed.

** Macroscopic failure of the F80 specimen before reaching 120 mm of displacement.

2.3. Swelling

Each sample is immersed in cyclohexane for 72 h and the solvent is replaced every 24 h. After 72 h, the swollen mass of each sample (m_s) is measured. The samples are then placed in a

vacuum oven at 70°C for 6 h to ensure the complete removal of the solvent. The mass of the dry samples (m_d) is then determined. The swelling ratio of the specimen (Q) was calculated following ref [20]. The network chain density is calculated from the swelling experiments and the Flory-Rehner equation [22]:

$$\upsilon = \frac{ln(1 - v_2) + v_2 + \chi_1 {v_2}^2}{V_1(-{v_2}^{\frac{1}{3}} + \frac{2}{f} v_2)} \quad (4)$$

With $v_2 = 1/Q_r$, V_1=108 cm^3/mol^{-1} is the molar volume of the solvent (cyclohexane), χ_1 is the Flory-Huggins polymer solvent dimensionless interaction term (χ_1 is equal to 0.353 for the EPDM-toluene system). The ratio *2/f* is associated with the phantom model that assumes spatial fluctuation of crosslinks (non-affine) used for high deformation ratios. *f*, the crosslink functionality, is chosen equal to 4. For filled compounds, the Kraus correction [23] is used to account for the contribution of filler in swelling ratio. Q_c is the swelling ratio of the rubber matrix defined as follows:

$$Q_c = \frac{Q - \phi}{1 - \phi} \quad (5)$$

with ϕ is the volume fraction of fillers. Krauss correction in Equation 5 assumes non-adhesion of the fillers to the rubbery matrix, suggesting damage in mechanically tested specimen may partly be ascribed to decohesion at filler-rubber interface.

2.4. Thermoporosimetry

EPDM samples are immersed into cyclohexane for 72 h to reach the swelling equilibrium. They are then carefully extracted and placed into aluminium crucibles. The thermoporosimetry experiments are performed using a Perkin Elmer Pyris diamond DSC. The sample is first cooled

down to -50°C at 10°C/min followed by an isothermal step at -50°C for 2 min. The sample is then heated at 10°C/min up to 30°C. The endothermic peaks observed in this heating scan correspond to the melting T_m of the cyclohexane entrapped in the network. Melting peaks are deconvoluted and the intensity is normalized by the swollen weight. The full procedure is described in references [24] and [25] on Natural Rubber materials and preliminary results had been obtained on EPDM specimens in reference [26]. By derivation of the Gibbs-Thompson equation, the normalized pore size is given by:

$$\frac{L}{L_f} = \frac{{T_m}^0 - T_f}{{T_m}^0 - T} \tag{6}$$

With T_f and L_f correspond to the melting temperature and the size of the largest pores entrapped in the network, respectively. After derivation of equation 6, the normalized intensity distribution of the pore size is given by:

$$I_n = \frac{1}{m}\frac{dH}{dT}\frac{\left({T_m}^0 - T\right)^2}{L_f} \tag{7}$$

It is important to note that the absolute value of L_f is not accessible from thermoporosimetry experiments. L_f value being unknown, the intensity $I=L_fI_n$ is hence plotted instead I_n to account for the pore size distribution. The average normalized pore size is then calculated as the L/L_f value associated with half of the area under the normalized signal.

2.5. Scanning electron microscopy (SEM)

A Carl Zeiss AG SUPRA 40 Scanning Electron Microscope (SEM) equipped with an in-lens detector is used to monitor fractured surfaces of specimens subjected to mechanical tests. Electrons are collected by in-lens detector. A working distance of 5 mm and an acceleration voltage of 3keV are chosen. To avoid charging effects, samples are carbon-coated prior to

analyses. A working distance of 9.9 mm is used to determine the chemical composition by Energy Dispersive X-Rays spectroscopy (EDXS).

2.6. Electrical resistivity

Resistivity is measured with a four-point contact method (Kelvin method) creating an arbitrary potential difference on the specimen via a generator. The current *I* and voltage *V* are measured by an ammeter (in series) and a voltmeter (in parallel) respectively, providing the specimen electrical resistance. The resistivity is calculated using the Ohm's law:

$$\rho = \frac{VS}{Il} \tag{8}$$

With *S* the cross section of the specimen and *l* the distance between voltmeter connectors. The electrical conductivity (in Siemens/m) is then calculated as the inverse of the resistivity.

3. Results and discussion

3.1. Macroscopic damage

The series of EPDM containing various filler contents has been first subjected to single loading and loading/unloading (Figure 2, Supplementary Figure S1). All specimens show hyper-viscoelastic behaviour with increasing mechanical dissipation with strain and filler content (Figure 2a, Supplementary Figure S1). However, the permanent strain only slightly increases with the maximum experienced strain and independently on filler content (Figure S2a) in spite of the larger local deformation in the presence of fillers. This indicates a high level of reversibility of the deformation mechanisms in filled specimens. The reinforcement effect of filler is shown on the stress strain curves (Figure 2a) where the elastic modulus and strength at failure increases with filler content. Such reinforcement is also clearly visible on the increased tangent modulus with filler content at moderate strains, i.e. up to λ=2 (Figure 2b). Volumetric strain, which

characterizes voids fraction in filler rubbers [6],[21], is found to significantly increase with filler content by reaching more than 50% for EPDM-80 at macroscopic failure (Figure 2c). Such high voids fraction might contribute to the stress release as observed in the loss of tangent modulus that precedes the macroscopic failure in EPDM-60 and EPDM-80 (Figure 2b).

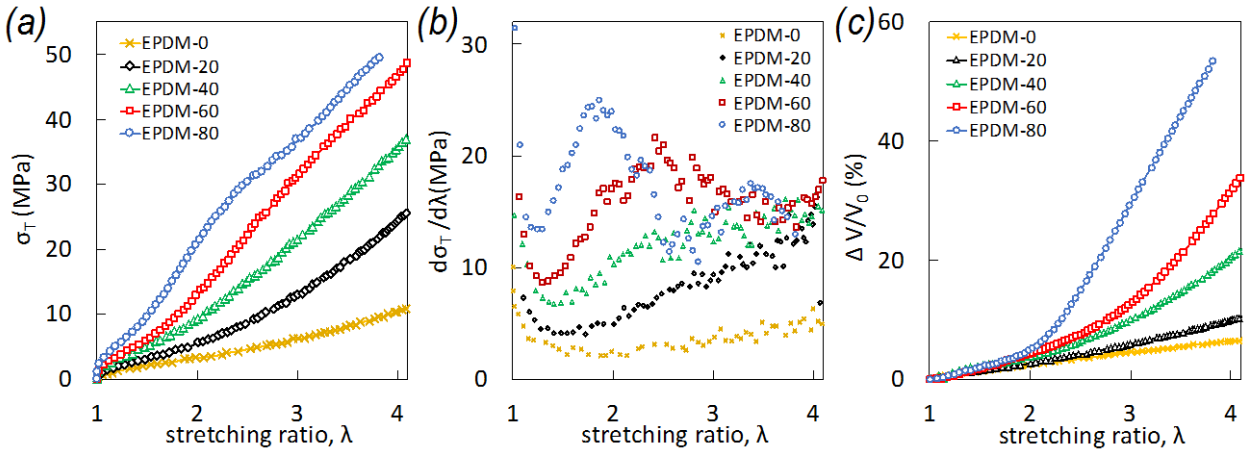

Figure 2. *(a)* True stress and *(b)* volumetric strain versus stretching ratio, *(c)* tangent modulus (calculated as the derivative of stress over strain) versus stretching ratio.

Additionally, volumetric strain loading-unloading curves show hysteresis associated with open loop in the unfilled EPDM-0 that is progressively closed by increasing filler content (Figure 3a-d). These results suggest that the presence of fillers favors the closing of voids upon unloading. This is confirmed by the high percentage of cavities closing in filled systems as compared to the unfilled one (Figure 3d). This percentage is defined as the difference between $\Delta V/V_0$ at λ_{max} and $\Delta V/V_0$ at the end of the unloading divided by $\Delta V/V_0$ at λ_{max}.

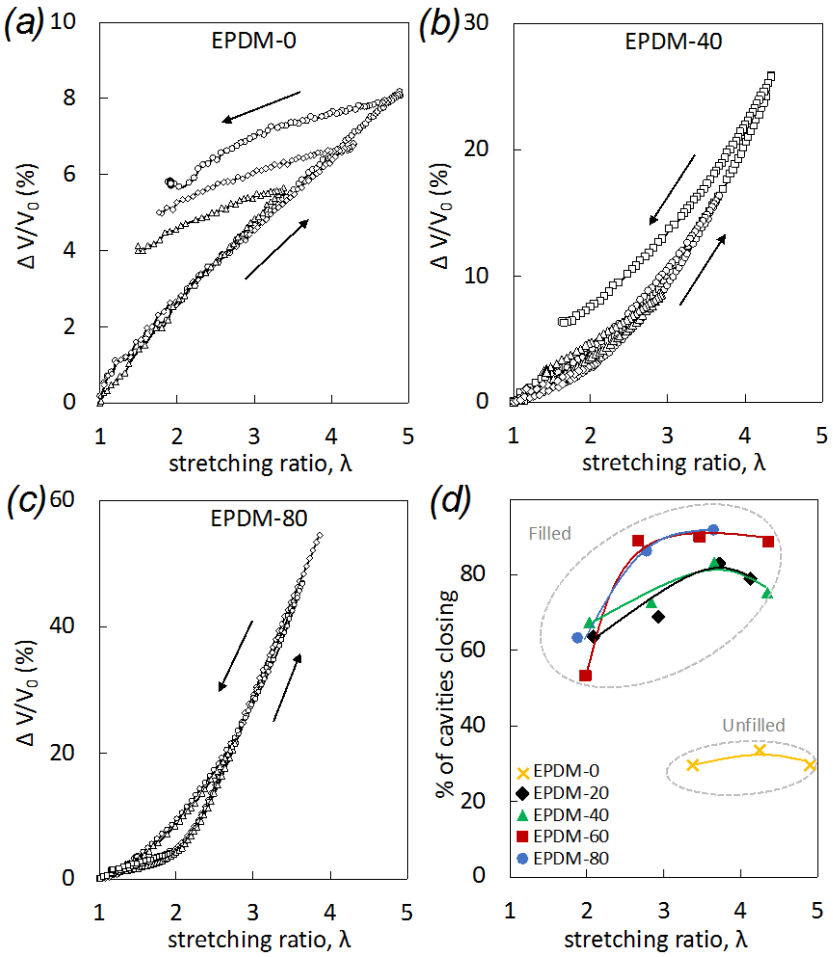

Figure 3. *(a,b,c)* Volumetric strain during uniaxial cyclic test performed on EPDM-0, EPDM-20, EPDM-40 and EPDM-80 respectively at room temperature and at the strain rate $1s^{-1}$. *(d)* Percentage of cavities closing (estimated as the division of the difference of volumetric strain at λ_{max} and at the end of unloading by the volumetric strain at λ_{max}). versus stretching ratio. A value of 100% means that all cavities open during loading were closed after unloading. Arrows indicate the loading/unloading directions.

3.2. Damage of the filler network

The previously observed irreversible volumetric strain in unfilled EPDM-0 (Figure 3d) is consistent with SEM images of fractured specimen showing thermally stable micro-voids. Contrarily, fractured surfaces in filled rubber (Figure 4b) show confined nano-voids between nanometric fillers aggregates. Such confinement is consistent with the presence of a 3D filler-

filler network of conducting phase in the undeformed state as shown by their high electrical conductivity (Figure 4c).

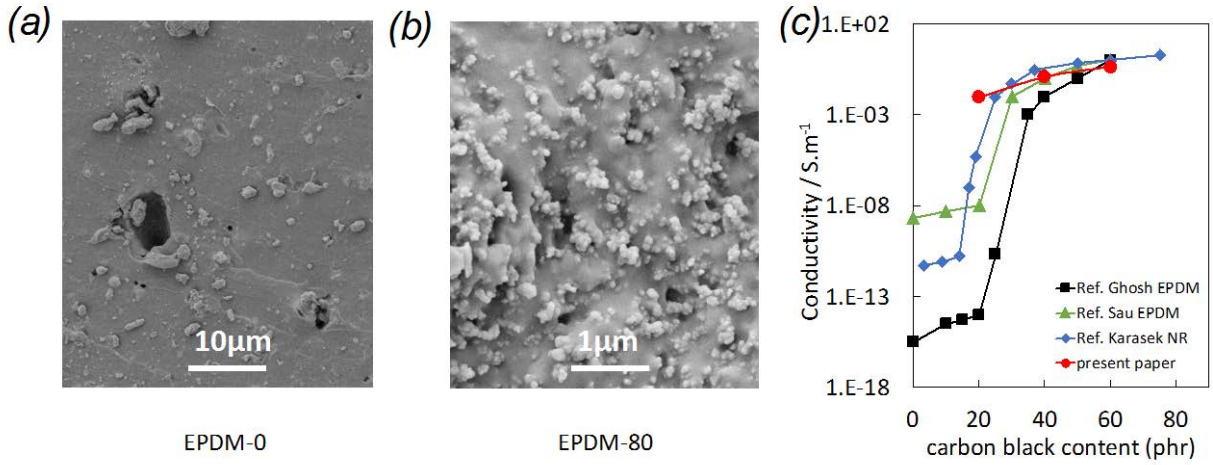

Figure 4. *(a),(b)* SEM images of cross-section of fractured EPDM-0 and EPDM-80 sample respectively, *(c)* Electrical conductivity versus carbon black content. The abrupt change in the conductivity is noted as the electrical percolation threshold, as shown in Refs. [27],[28],[29].

The presence of the filler network of conducting phase may arise from the flocculation, i.e. the rearrangement of carbon black particles that lead to the formation of continuous aggregates of carbon black particles. Flocculation occurs after the mixing process, when both rubber and fillers rearrange, leading to the re-agglomeration of the filler network. The dynamics of such mechanism [30] and the effect of heat treatment [31],[32],[33] have been extensively studied in carbon black filled EPDM. The transition from dispersed phase to flocculated phase may lead to the observed conductivity jump as observed in [27],[28],[29] and in Figure 4c.

While the filler-filler network and its associated reinforcement effect vanish above the linear elastic regime due to Payne's effect [34], filler-filler network is expected to re-arrange via re-aggregation [17],[35],[36],[37] at larger strain. This re-arrangement may contribute to localize cavitation in the vicinity of the filler aggregates owing the load bearing capacity of the filler-filler network. Such localized cavitation suggests the immobilized rubber phase, namely both

occluded rubber into the aggregates and bound rubber at the filler interface, to play an important role in damage mechanisms.

To identify the potential contribution of occluded and bound rubber, an analysis of the reinforcement effect of the fillers on large strain elastic properties is conducted (Figure 5). The experimental variation of the elastic modulus with the filler content is compared to different theoretical models: hydrodynamic model, occluded and bounded rubber models as detailed in the legend of figure 5. Experimental large strain elastic modulus (10%) deduced from the Gaussian approximation follows the theoretical value estimated from the hydrodynamic amplification factor [38] up to a critical filler content φ_c=40 phr (Figure 5). However, it diverges beyond, with a mechanical reinforcement suggesting the immobilized rubber to have a role in mechanical reinforcement. First, occluded rubber fills the void within each aggregate and does not contribute to the matrix deformation [39]. Secondly, bound rubber may form a shell surrounding the aggregates [40], [41]. Hence, both occluded and bound rubber may increase the apparent filler volume fraction yielding to supplementary sources of elastic reinforcement. Experimental data even surpasses theoretical trends in the case of EPDM-80, suggesting this material to likely contain both occluded and bound rubber taking part into the elastic reinforcement.

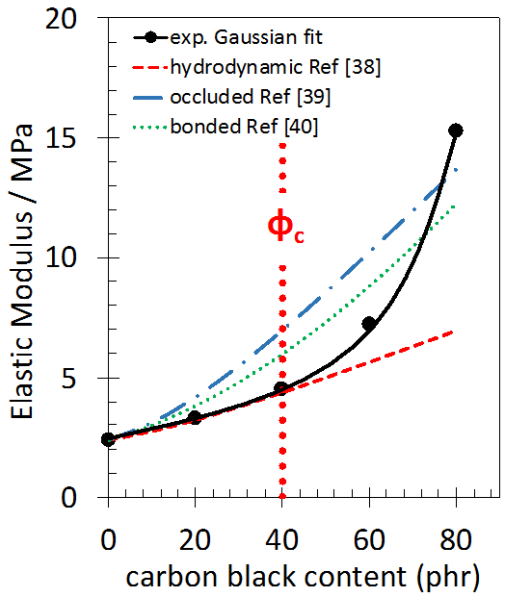

Figure 5. Comparison of the experimental elastic modulus versus filler content and theoretical predictions. Elastic modulus calculated from Gaussian approximation $\sigma=E/3(\lambda-1/\lambda^2)$ (data points) at 10% strain. Theoretical filler content dependence of elastic modulus obtained from the hydrostatic factor following Guth [38], $E/E_0 = 1 + 2.5\phi + 14.1\phi^2$, with E_0 the modulus of the unfilled EPDM, and ϕ the filler content (vol.%) (red dotted line). Theoretical elastic modulus corrected to account for the occluded rubber following Ref. [39] (blue dashed dotted line) associated with the effective volume of filler $\phi_{eff} = (1 + 0.0214\, DBPA)/1.46$, with DBPA=120 is the dibutyl phthalate absorption number of the carbon black N550. Theoretical elastic modulus corrected to account for the presence of immobilized bound rubber (green dotted line) as described in Ref. [40] in the form of a shell: $\phi_{sh}/\phi_{agg} = \left[(r + \phi_{sh})^3 - r^3\right]/r^3$, where ϕ_{sh} is the volume fraction of shell rubber, r is the radius of equivalent surface area of an aggregate and r_{sh} is the thickness of partially immobilised shell rubber on the surface of aggregates. The thickness of shell rubber is chosen equal to 2.5 nm.

In vulcanized rubber, not only the filler network and associated immobilized rubber may be damaged. The chains in the rubbery matrix far from filler surface are elastically active due to entanglements and sulphur bonds and expected to experience some damage upon deformation via chains scission and/or sulphur bonds breakage. In the following, the contribution of damage in the rubbery network is distinguished from the one in the filler-filler network and its dependence on the filler content and on the applied strain is investigated.

3.3. Damage of the rubber network

Damage of chains network in the rubber matrix, i.e. the breakage of elastically active bonds, is accessible via an evaluation of the network chains density, ν, within applied strain. In a first step, the undamaged network chains density of the series of EPDM is performed on undeformed specimens. In a second step, the effect of the strain on the network chains density is performed after performing loading-unloading at various maximum deformations.

For undeformed specimens, the network chains density of the unfilled EPDM is calculated by using swelling ratio and Flory-Rehner equation (see section 2.3). The average value of the network chain density in filled rubbers is then deduced from thermoporosimetry experiments and explained as follows.

In thermoporosimetry, the melting behaviour of crystallized swollen EPDM specimen is characterized by three endothermic peaks: $T_{m,1}$ and $T_{m,2}$ due to trapped solvent and $T_m^0 = 10°C$ the melting temperature of free solvent (Figure 6a). The intensity of the peak maximum at $T_{m,1}$ increases in detriment to the one of $T_{m,2}$ by increasing the filler content. This indicates a decrease of swollen pore size. After deconvolution of the melting peaks (see procedure in references [20],[42]), the use of equations (6) and (7) in section 2.4 provides access to the pore size distribution. The normalized pore size L/L_f shows large distribution (Figure 6b), as expected in both filled and unfilled vulcanized EPDM [43]. The characteristic distance of chains network r in the un-swollen state can then be inferred from the pore size L via the relation $L = Q^{1/3}r$, with r the root-mean-square end-to-end distance $\sqrt{\langle R^2 \rangle}$ between nodes of the chains network. Assuming Gaussian chains statistics for the calculation of r, it comes $\langle R^2 \rangle = C_\infty n l^2$ with $C_\infty = 6.62$ [44] is the number of backbone bonds in one EPDM statistical segment, n is the average number of backbone bonds per monomer unit and l =2 Å is the average main-chain bond length. $n = M/M_0$ with $M = \rho/\nu$ and M_0 =35 g.mol^{-1} the weight-average molar mass of the

network chains and of the monomer respectively. ρ =0.865 g.cm^{-3} is the bulk rubbery density and ν (mol.cm^{-3}) is the network chains density. The average distance between nodes of the chains network can then be given by:

$$r = \left(\frac{C_\infty \rho}{\nu M_0}\right)^{1/2} l \tag{9}$$

The average swollen normalized pore size $(L/L_f)_a$, is calculated as the pore size value corresponding to half of the area of the intensity distribution in Figure 6b. From Eq. (9), the relation between ν and average pore size can be expressed as:

$$\left(\frac{L}{L_f}\right)_a Q^{-1/3} = K\nu^{-1/2} \tag{10}$$

with K a constant equal to $(C_\infty \rho/M_0)^{1/2} l/L_f$. Equation (10) assumes Gaussian approximation. Assuming that swelling leads to equiaxial reopening of the cavities, equation (2) adapted to swelling can be given as $\Delta Q/Q_0 = \lambda^3 - 1$. In our materials, the maximum swelling ratio Q_r = 3.9 (Figure 6a) corresponds to a maximum stretching ratio of λ = 1.6 for unfilled rubber, and λ = 1.3 in EPDM with highest filler content (EPDM-80) in the swollen state, which belongs to the Gaussian elastic regime in the same specimen (Figure 2). Equation (10) applied to both filled and unfilled EPDM yields to:

$$\nu_c = \nu \left(\frac{L_c}{L}\right)^2 \left(\frac{Q_c}{Q}\right)^{2/3} \tag{11}$$

with Q_c, L_c and ν_c are the swelling ratio, the average swollen pore size and the average network chains density of the filled EPDM respectively, and Q, L and ν are the same parameters for the unfilled EPDM. Q_c is calculated using equation (5) in section 2.3. From equation (11), the

average network chain density is found to slightly increase with carbon black content (Figure 6c) suggesting only slight contribution of the immobilized rubber chains at filler interface, as measured from thermoporosimetry.

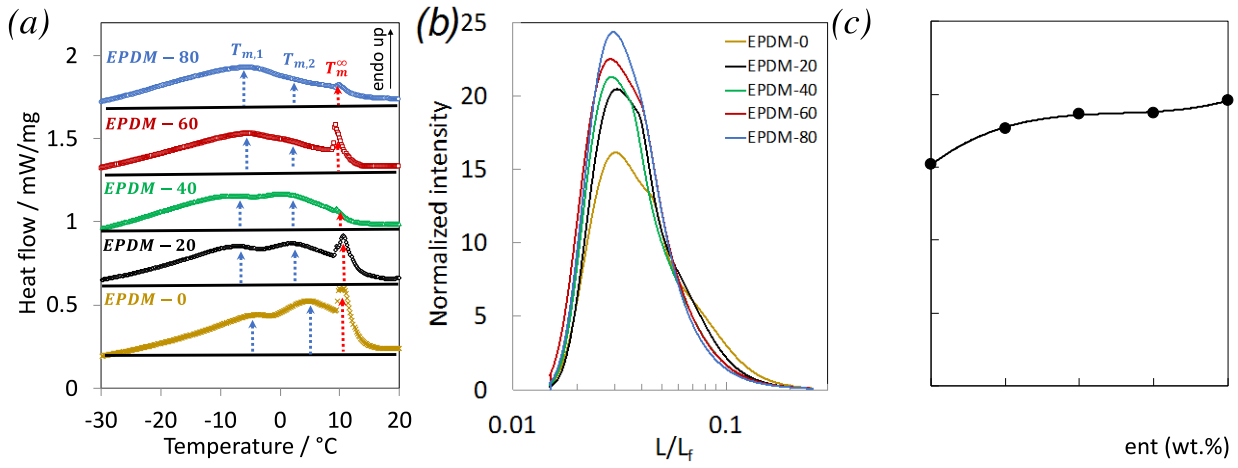

Figure 6. *(a)* DSC thermoporosimetry heating for undeformed EPDM-0, EPDM-20, EPDM-40, EPDM-60 and EPDM-80. Blue dotted arrows indicate the trapped solvent melting peaks ($T_{m,1}$ and $T_{m,2}$) and red dotted arrows indicate the free solvent melting peak, *(b)* Normalized intensity versus normalized pore size giving the pore size distribution (see section 2.4), *c)* Network chain densities of filled EPDM calculated from equation (11).

The effect of strain on chains network damage in filled EPDM is now investigated by performing swelling experiments on specimen previously stretched at various strains. Swelling ratio Q is found to increase with applied strain with a more pronounced effect in filled rubber compared to unfilled one (Figure 7a). Like for DIC volumetric strain, a volumetric strain for swelling experiments $\Delta Qc/Qc_0$ is defined as $\Delta Qc(\lambda)/Qc_0 = (Qc(\lambda) - Q_0)/Q_0$ where $Q(\lambda)$ denotes the swelling ratio of a filled specimen mechanically tested up to λ and $Qc_0 = Qc(\lambda = 1)$ is the swelling ratio of a virgin specimen (un-stretched). The relation $Q_r = KQ_c$ is preserved with applied strain assuming decohesion at filler-rubber interface to occur during swelling in both undeformed and deformed specimens. Such relation being assumed, volumetric strain obtained from swelling of the filled rubber $\Delta Qc(\lambda)/Qc_0$ and of the rubber $\Delta Q(\lambda)/Q_0$ are expected to be similar.

Volumetric strain obtained by swelling indeed follows the same trend with the one obtained by DIC, up to a critical value around 10% (Figure 7b). However, above the critical value, volumetric strain estimated from swelling is lower than the one measured by DIC. The latter reaches larger values, especially in highly filled EPDM stretched at largest strain.

Assuming macroscopic voiding to be fully described by the alteration of elastically active chains, the network chains density ν of the deformed specimens can be obtained by combining swelling experiment and Flory-Rehner equation. All samples show a decrease of ν with strain (data points in Figure 7c). Network chain density obtained by DIC is calculated from the DIC volumetric strain and Flory-Rehner equation, via the relation:

$$v_2 = \frac{1}{Q_r} = \frac{1}{Q_{0,r}\left(1 + \frac{\Delta V}{V_0}\right)} \tag{12}$$

Results presented in Figure 7c (lines) show a decrease of the network chains density with strain. For lowest filler content (0 and 20 phr) consistency between chains network decrease obtained by swelling and DIC methods suggest the assumption of damage ascribed to chains network in the rubber phase to be realistic. This is consistent with the network alteration theory suggesting that a major strain induced damage mechanism in filled elastomers is associated with covalent bonds breakage in the rubber network as chains extend until their limit [45],[46],[47]. Contrarily, in highly filled rubbers ($\varphi > \varphi_c$), chains network alteration deduced from DIC becomes higher with strain than the one measured by swelling. Such discrepancies may arise from the dominance of damage mechanisms in highly filled EPDM that prevents the chains network alteration. Such mechanism occurs above a certain critical strain that decreases with the filler content (Figure 7d). Indeed, the decrease of ν with strain measured by DIC may be overestimated as it does not account for the damage associated with the filler network involving bound and occluded rubber

chains. Contrarily, the network chains alteration from swelling may be underestimated due to re-arrangement of 3D filler network as discussed in section 3.2. Such re-arrangement favours cavities closing during unloading and prevents subsequent re-opening of cavities upon swelling. Hence, swelling and DIC methods may represent the lower and upper limits of the elastically active chains network alteration effect, respectively. The critical strain, λ_c, that describes the strain transition from chains network to filler network damage is deduced from the value at which the strain dependent curves of the network chain density (Figure 7c) deviate from each other. In highly filled EPDM above a critical strain (Figure 7a), macroscopic voiding is dominated by filler network damage, such damage being highly reversible as previously shown during single loading-unloading (section 3.1). This reversible behaviour is further discussed in the following section by extending our investigations to cyclic mechanical loadings.

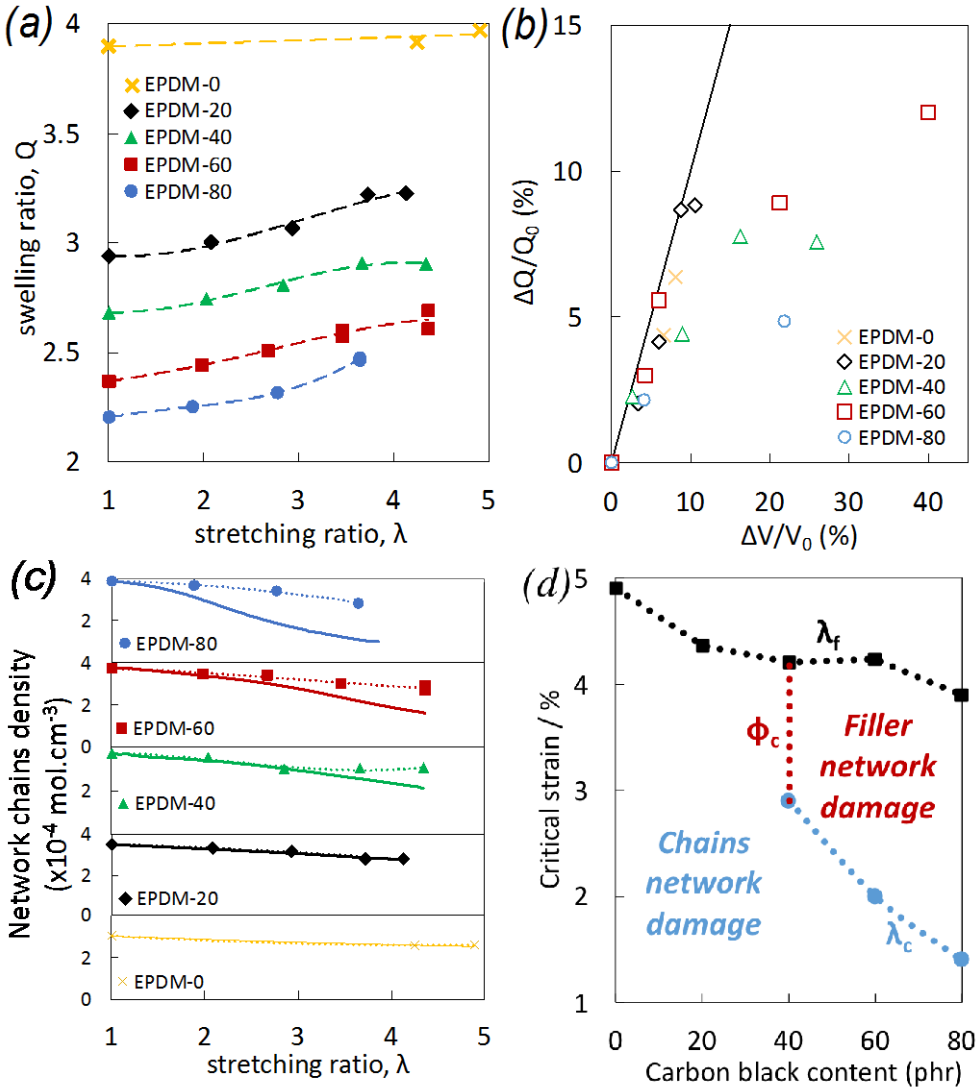

Figure 7. *(a)* Swelling ratio versus maximum stretching ratio that specimens have undergone during mechanical testing. Dotted lines are guides for the eyes. *(b)* Relative swelling ratio calculated from figure 7a versus DIC volumetric strain. The continuous line is a plot of $\Delta Q/Q_0 = \Delta V/V_0$. *(c)* ν estimated by swelling (data points and dotted lines) versus maximum stretching ratio. ν calculated by DIC volumetric strain is plotted with continuous lines. *(d)* Mapping of the major damage mechanisms occurring in the series of EPDM depending on the filler content and the applied strain. λ_c is the critical strain that separate the two major damage mechanisms dominated by chains network alteration and filler network damage. λ_f is the strain at macroscopic failure.

3.4. Damage during multiple loading/unloading

To access more realistic loading conditions seen in industrial processes, e.g. mechanical devulcanization, damage behavior is characterized during multiple cycles (Figures 8-10). Specimens are cyclically stretched up to incremental λ_{max}. Specimens are stretched five times at each λ_{max}. For sake of clarity, only the loading-unloading curves (Figures 8ac and Figure 9a-c) obtained for the first cycle for each λ_{max} is plotted (full series of data available in Supplementary Figure S3, S4). Additionally, data measured for the five cycles at each λ_{max} are presented (in Figures 8 d-f and Figure 9 d-f). The first cycles for each λ_{max} in filled EPDM show large hysteresis loop (Figure 8b and Figure 8c). This traduces high mechanical dissipation (Figure S5b,c) that decreases after the first cycle and stabilizes for the subsequent cycles at any λ_{max}. The stress at the various λ_{max} also first decreases and then stabilizes (Figure 8e and Figure 8f), suggesting Mullins softening. Unfilled EPDM also shows a decrease of dissipated energy (Figure S5a), but no stress softening (Figure 8d). When λ surpasses λ_{max} the stress tends to follow the single tensile test curve, except for EPDM-80 that shows a slight increase of both stress and strain at break in EPDM-80, consistent with the contribution of Mullins effect to increase resistance to cyclic loading [48].

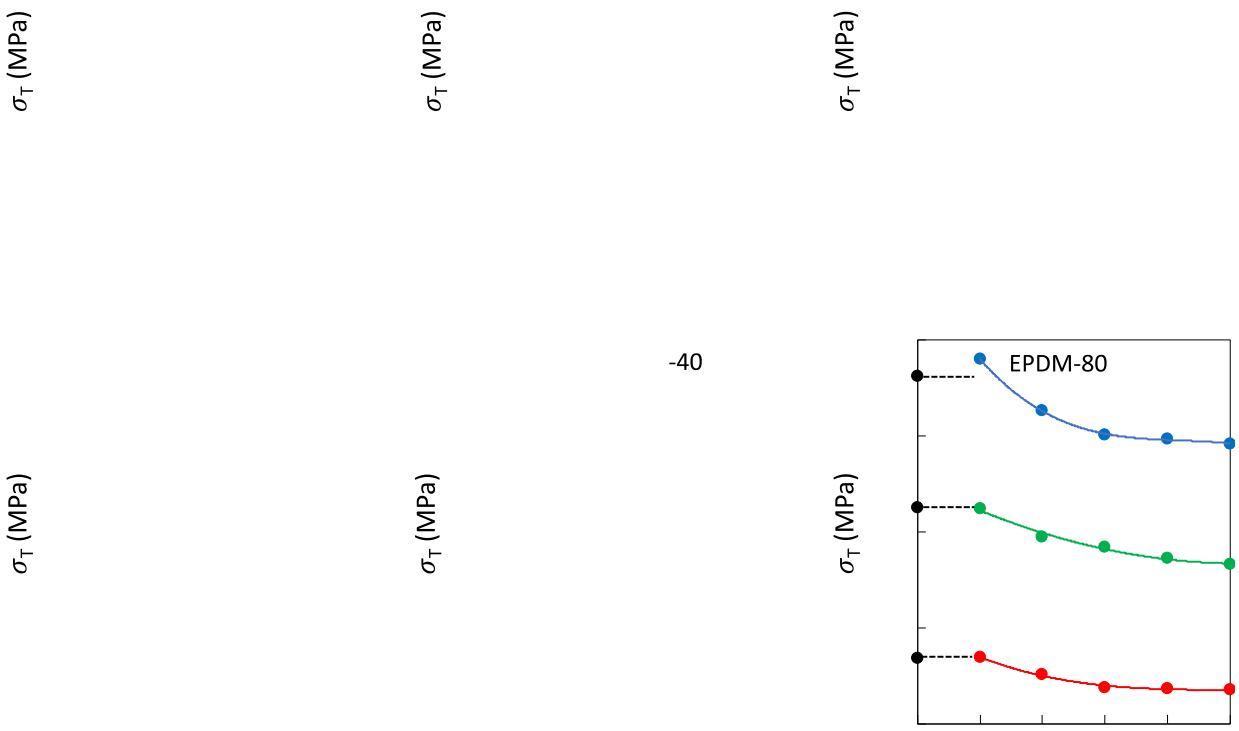

Figure 8. True stress versus stretching ratio for EPDM-0 *(a)*, EPDM-40 *(b)* and EPDM-80 *(c)* respectively during multiple cyclic loadings performed at three different stretching ratios λ_1 (in red), λ_2 (in green) and λ_3 (in blue). Only the first cycles for each λ is given (full stress-strain curves in Figure S4). True stress at λ_{max} versus the number of cycles at λ_1 (in red), λ_2 (in green) and λ_3 (in blue) for EPDM-0 *(d)*, EPDM-40 *(e)* and EPDM-80 *(f)* respectively during same multiple cyclic loading.

The volumetric strain of the unfilled EPDM-0 shows weak dependence on strain (Figure 9a), and no dependence on cycles accumulation (Figure 9d). EPDM-40 (Figure 9b) and EPDM-80 (Figure 9c) both show increased volumetric strain with increased λ_{max}. No effect of cycles accumulation is observed in EPDM-40 (Figure 9e). EPDM-80 shows a strong decrease in volumetric strain which stabilizes after the third cycle (Figure 9f), resulting in a significant delay of volumetric strain compared to single loading. This confirms a certain ability to accommodate damage, that subsequently improves the resistance to failure as previously commented on Figure 8c. Another feature of Mullins effect is its anisotropy. In pre-stretched specimen, Mullins softening is higher in the direction parallel to the pre-stretch than the orthogonal one [46] [49]. Such effect may be related to the anisotropization of the fillers aggregates [50]. The latter is described by the damage anisotropy factor, *A*, obtained from equation (3) as shown in section 2.2. The dependence of the anisotropy factor, A, is similar to that of voids fraction on strain (Figure S6) and cyclic accumulation (Figure S7). Thus, increased voids fraction is not only ascribed to an increasing number of isotropic voids nuclei initially subjected to triaxial stresses as confined in between fillers aggregates, but also to their subsequent growth in the stretching direction. Additionally, decreased volumetric strain in cyclic test compared to single test in highly filled rubber is accompanied by the significant decrease of damage anisotropy factor that is consistent with the closing of cavities favoured by cyclic accumulation.

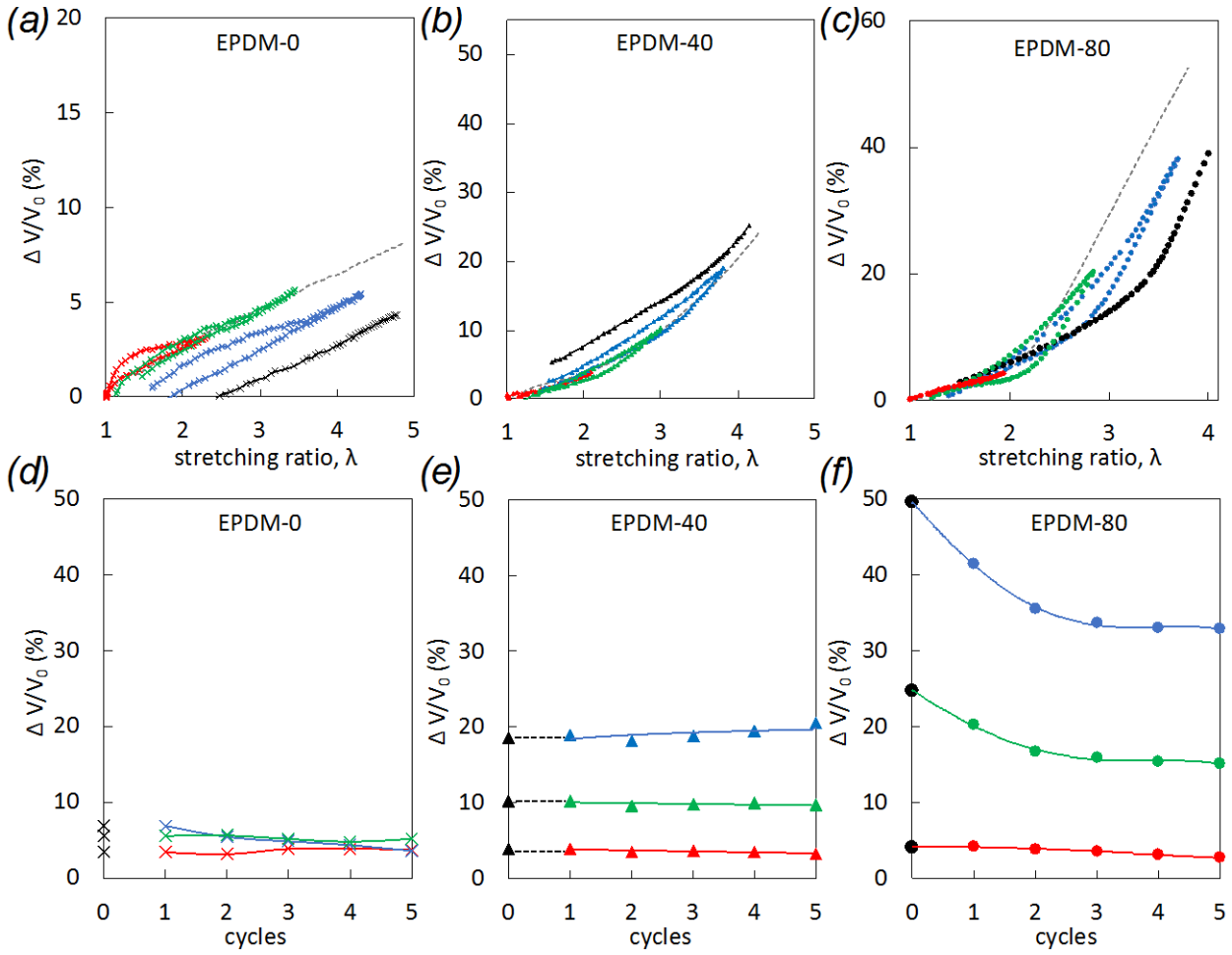

Figure 9. Volumetric strain versus stretching ratio for EPDM-0 *(a)*, EPDM-40 *(b)* and EPDM-80 *(c)* respectively during multiple cyclic loadings performed at three different stretching ratios λ_1 (in red), λ_2 (in green) and λ_3 (in blue). Only the first cycles at each λ is given (see full data in Figure S6). True stress versus the number of cycles at λ_1 (in red), λ_2 (in green) and λ_3 (in blue) for EPDM-0 (d), EPDM-40 **(e)** and EPDM-80 *(f)* respectively during same multiple cyclic loading.

The differences in large strain mechanisms and Mullins damage between low and high filler content regions are now discussed based on the full series of EPDM containing 0, 20, 40, 60 and 80 phr of fillers (Figure 10). Above the critical filler content of 40 phr, the volumetric strain (Figure 9a) and anisotropy factor (Figure 10b) decrease significantly after cyclic loadings as compared to single one. Above the same threshold filler content, the network chain density deduced from DIC is found to be higher after cyclic accumulation, in comparison to single loading (Figure 10c). This trend is further confirmed by the calculation of the network chain

density obtained from swelling experiments (Figure 10c). Mullins softening has been described not only to be resulted from the damage of 3D filler network [37], but also related to the release of both occluded rubber [51] and bound rubber [52]. Filler-filler rupture associated with voiding inside the fillers aggregates and in the vicinity of the fillers may indeed, in turn, release the bound rubber at the filler-rubber interface and the occluded rubber into the filler aggregates. This would contribute to delay further increase of both volumetric strain and anisotropy factor during cyclic accumulation. Hence, cycles accumulation prevents both nucleation and growth of cavities in the rubber matrix, yielding to a decrease in chains network alteration in filled rubbers with filler content > 40 phr as compared to single loadings.

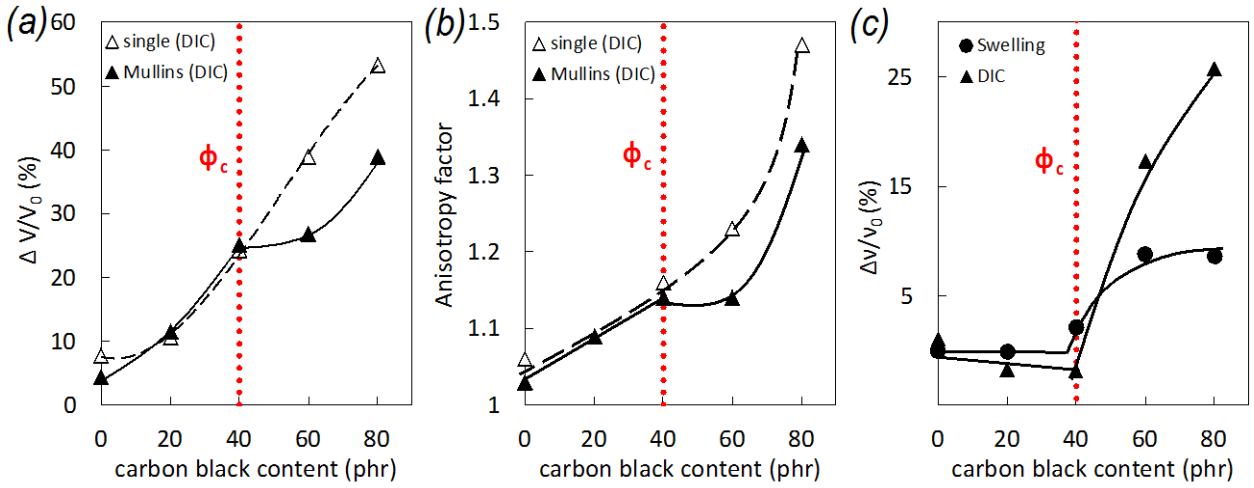

Figure 10. *(a)* DIC volumetric strain versus filler content for single and Mullins type tests measured at maximum strain, *(b)* corresponding anisotropy factor, *(c)* network chains density measured from swelling (Q) and DIC (V) for EPDM-0, EPDM-40 and EPDM-80 in undeformed state and stretched up to maximum extension.

4. Conclusion

In this paper, damage mechanisms in vulcanized carbon black filled EPDM subjected to both single and multiple cyclic tensile tests are examined. This has been conducted by the combination of *in-situ* characterization of macroscopic voids via Digital Image Correlation (DIC) and *ex-situ* characterization of chains network alteration via swelling experiments. From this multi-scale approach, the contributions of (I) *the filler network* (filler-filler bonds), (II) *the immobilized rubber* (occluded/bonded to filler) and (III) *the elastically active rubber chains* (crosslinked, entangled) have been identified.

Below 40 phr of fillers, damage mechanisms mostly occur in the elastically active rubber chains network by chains scission and/or sulfur bond breakage. At and above 40 phr of fillers, damage first occurs in the elastically active rubber network, but by increasing the strain, the filler network then re-organizes (re-aggregation) and bears the load, yielding to localized damage in the vicinity of the fillers. As a result, rubber bonded at filler interface and occluded rubber into the filler aggregates may be released. Such partially reversible release involving loss of weak molecular interactions (chains slip, physical bond breakage) prevents further development of irreversible cavities in the elastically active rubber phase during Mullins type tests.

In future works, it may be interesting to apply our approach to provide an insight into damage mechanisms in various rubbers subjected to even more realistic loading conditions. As an example, cyclic shear deformation may be applied to properly mimic mechanical devulcanization during the high-shear mixing process [1], [53], [54] which is of significance for the recycling of waste rubbers.

5. Acknowledgements

The authors are indebted to the company SACRED for providing the rubber gum and to the laboratory GEPEA of the University of Nantes for the curing procedure of rubber materials. This work was performed within the framework of the project ECOTHER supported by BPiFrance.

6. References

[1] R. Diaz, G. Colomines, E. Peuvrel-Disdier, et R. Deterre, « Thermo-mechanical recycling of rubber: Relationship between material properties and specific mechanical energy », *J. Mater. Process. Technol.*, vol. 252, p. 454‑468, 2018, doi: 10.1016/j.jmatprotec.2017.10.014.

[2] M. a. L. Verbruggen, L. van der Does, J. W. M. Noordermeer, M. van Duin, et H. J. Manuel, « Mechanisms Involved in the Recycling of NR and EPDM », *Rubber Chem. Technol.*, vol. 72, n° 4, p. 731‑740, 1999, doi: 10.5254/1.3538830.

[3] W. V. Mars et A. Fatemi, « Factors that Affect the Fatigue Life of Rubber: A Literature Survey », *Rubber Chem. Technol.*, vol. 77, n° 3, p. 391‑412, 2004, doi: 10.5254/1.3547831.

[4] J. a. C. Harwood, L. Mullins, et A. R. Payne, « Stress softening in natural rubber vulcanizates. Part II. Stress softening effects in pure gum and filler loaded rubbers », *J. Appl. Polym. Sci.*, vol. 9, n° 9, p. 3011‑3021, 1965, doi: 10.1002/app.1965.070090907.

[5] J. Ramier, C. Gauthier, L. Chazeau, L. Stelandre, et L. Guy, « Payne effect in silica-filled styrene–butadiene rubber: Influence of surface treatment », *J. Polym. Sci. Part B Polym. Phys.*, vol. 45, n° 3, p. 286‑298, 2007, doi: 10.1002/polb.21033.

[6] Y. Merckel, J. Diani, M. Brieu, et J. Caillard, « Effects of the amount of fillers and of the crosslink density on the mechanical behavior of carbon-black filled styrene butadiene

rubbers », *J. Appl. Polym. Sci.*, vol. 129, n° 4, p. 2086‑2091, 2013, doi: 10.1002/app.38925.

[7] J. L. W. Carter, M. D. Uchic, et M. J. Mills, « Impact of Speckle Pattern Parameters on DIC Strain Resolution Calculated from In-situ SEM Experiments », in *Fracture, Fatigue, Failure, and Damage Evolution, Volume 5*, 2015, p. 119‑126.

[8] F. Hild, S. Roux, et E. Eikologie, « Ten years of global digital volume correlation: What has been achieved? », in *International Conference on Nonlinear Solid Mechanics*, Rome, Italy, 2019.

[9] J. de Crevoisier *et al.*, « Volume changes in a filled elastomer studied via digital image correlation », *Polym. Test.*, vol. 31, n° 5, p. 663‑670, 2012, doi: 10.1016/j.polymertesting.2012.04.003.

[10] L. Chen *et al.*, « Unveiling Reinforcement and Toughening Mechanism of Filler Network in Natural Rubber with Synchrotron Radiation X-ray Nano-Computed Tomography », *Macromolecules*, vol. 48, n° 21, p. 7923‑7928, 2015, doi: 10.1021/acs.macromol.5b01301.

[11] H. Zhang *et al.*, « Opening and Closing of Nanocavities under Cyclic Loading in a Soft Nanocomposite Probed by Real-Time Small-Angle X-ray Scattering », *Macromolecules*, vol. 46, n° 3, p. 900‑913, 2013, doi: 10.1021/ma302325w.

[12] J. Ramier, L. Chazeau, C. Gauthier, L. Stelandre, L. Guy, et E. Peuvrel-Disdier, « In situ SALS and volume variation measurements during deformation of treated silica filled SBR », *J. Mater. Sci.*, vol. 42, n° 19, p. 8130‑8138, 2007, doi: 10.1007/s10853-007-1728-1.

[13] N. Suzuki, M. Ito, et F. Yatsuyanagi, « Effects of rubber/filler interactions on deformation behavior of silica filled SBR systems », *Polymer*, vol. 46, n° 1, p. 193‑201, 2005, doi: 10.1016/j.polymer.2004.10.066.

[14] J. M. Clough, C. Creton, S. L. Craig, et R. P. Sijbesma, « Covalent Bond Scission in the Mullins Effect of a Filled Elastomer: Real-Time Visualization with Mechanoluminescence », *Adv. Funct. Mater.*, vol. 26, n° 48, p. 9063‑9074, 2016, doi: 10.1002/adfm.201602490.

[15] F. Bueche, « Molecular basis for the mullins effect », *J. Appl. Polym. Sci.*, vol. 4, n° 10, p. 107‑114, 1960, doi: 10.1002/app.1960.070041017.

[16] R. Houwink, « Slipping of Molecules during the Deformation of Reinforced Rubber », *Rubber Chem. Technol.*, vol. 29, n° 3, p. 888‑893, 1956, doi: 10.5254/1.3542602.

[17] G. Kraus, C. W. Childers, et K. W. Rollmann, « Stress softening in carbon black-reinforced vulcanizates. Strain rate and temperature effects », *J. Appl. Polym. Sci.*, vol. 10, n° 2, p. 229‑244, 1966, doi: 10.1002/app.1966.070100205.

[18] D. E. Hanson *et al.*, « Stress softening experiments in silica-filled polydimethylsiloxane provide insight into a mechanism for the Mullins effect », *Polymer*, vol. 46, n° 24, p. 10989‑10995, 2005, doi: 10.1016/j.polymer.2005.09.039.

[19] N. Candau, J-L. Bouvard, E. Peuvrel-Disdier, R. Valette, C. Pradille, et al.. «Coupled thermal and volume change measurements during stretching of filled EPDM rubbers». 10th International Conference on Mechanics of Time-Dependent Materials (MTDM2016), 2016, Paris, France. hal-01499444.

[20] N. Candau, O. Oguz, E. Peuvrel-Disdier, J.-L. Bouvard, C. Pradille, et N. Billon, « Strain-induced network chains damage in carbon black filled EPDM », *Polymer*, vol. 175, p. 329‑338, 2019, doi: 10.1016/j.polymer.2019.05.017.

[21] N. Candau, C. Pradille, J.-L. Bouvard, et N. Billon, « On the use of a four-cameras stereovision system to characterize large 3D deformation in elastomers », *Polym. Test.*, vol. 56, p. 314‑320, 2016, doi: 10.1016/j.polymertesting.2016.10.017.

[22] P. J. Flory et J. R. Jr, « Statistical Mechanics of Cross-Linked Polymer Networks I. Rubberlike Elasticity », *J. Chem. Phys.*, vol. 11, n° 11, p. 512‑520, nov. 1943, doi: 10.1063/1.1723791.

[23] G. Kraus, « Swelling of filler-reinforced vulcanizates », *J. Appl. Polym. Sci.*, vol. 7, n° 3, p. 861‑871, 1963, doi: 10.1002/app.1963.070070306.

[24] N. Candau *et al.*, « Strain-Induced Crystallization of Natural Rubber and Cross-Link Densities Heterogeneities », *Macromolecules*, vol. 47, n° 16, p. 5815‑5824, 2014, doi: 10.1021/ma5006843.

[25] N. Candau, L. Chazeau, J.-M. Chenal, C. Gauthier, et E. Munch, « Complex dependence on the elastically active chains density of the strain induced crystallization of vulcanized natural rubbers, from low to high strain rate », *Polymer*, vol. 97, p. 158‑166, 2016, doi: 10.1016/j.polymer.2016.05.020.

[26] N. Candau, J-L. Bouvard, E. Peuvrel-Disdier, R. Valette, N. Billon. Effect of stretching on the network structure of carbon black filled EPDM rubbers. 16th Conference Elastomery (Elastomery 2015), 2015, Tours, France. 2 p. hal-01502249.

[27] P. Ghosh et A. Chakrabarti, « Conducting carbon black filled EPDM vulcanizates: assessment of dependence of physical and mechanical properties and conducting character

on variation of filler loading », *Eur. Polym. J.*, vol. 36, n° 5, p. 1043‑1054, 2000, doi: 10.1016/S0014-3057(99)00157-3.

[28] L. Karásek et M. Sumita, « Characterization of dispersion state of filler and polymer-filler interactions in rubber-carbon black composites », *J. Mater. Sci.*, vol. 31, n° 2, p. 281‑289, 1996, doi: 10.1007/BF01139141.

[29] K. P. Sau, T. K. Chaki, et D. Khastgir, « Electrical and mechanical properties of conducting carbon black filled composites based on rubber and rubber blends », *J. Appl. Polym. Sci.*, vol. 71, n° 6, p. 887‑895, 1999, doi: 10.1002/(SICI)1097-4628(19990207)71:6<887::AID-APP4>3.0.CO;2-D.

[30] J. G. Meier et M. Klüppel, « Carbon Black Networking in Elastomers Monitored by Dynamic Mechanical and Dielectric Spectroscopy », *Macromol. Mater. Eng.*, vol. 293, n° 1, p. 12‑38, 2008, doi: 10.1002/mame.200700228.

[31] B. Wessling, « Electrical conductivity in heterogeneous polymer systems. V (1): Further experimental evidence for a phase transition at the critical volume concentration », *Polym. Eng. Sci.*, vol. 31, n° 16, p. 1200‑1206, 1991, doi: 10.1002/pen.760311608.

[32] K. P. Sau, T. K. Chaki, et D. Khastgir, « Carbon fibre filled conductive composites based on nitrile rubber (NBR), ethylene propylene diene rubber (EPDM) and their blend », *Polymer*, vol. 39, n° 25, p. 6461‑6471, 1998, doi: 10.1016/S0032-3861(97)10188-4.

[33] K. P. SAU, T. K. CHAKI, et D. KHASTGIR, « Conductive rubber composites from different blends of ethylene-propylene-diene rubber and nitrile rubber », *J. Mater. Sci.*, vol. 32, n° 21, p. 5717‑5724, 1997, doi: 10.1023/A:1018613600169.

[34] J. Fröhlich, W. Niedermeier, et H.-D. Luginsland, « The effect of filler–filler and filler–elastomer interaction on rubber reinforcement », *Compos. Part Appl. Sci. Manuf.*, vol. 36, n° 4, p. 449‑460, 2005, doi: 10.1016/j.compositesa.2004.10.004.

[35] V. Jha, A. G. Thomas, M. Bennett, et J. J. C. Busfield, « Reversible electrical behavior with strain for a carbon black-filled rubber », *J. Appl. Polym. Sci.*, vol. 116, n° 1, p. 541‑546, 2010, doi: 10.1002/app.30556.

[36] W. Fu *et al.*, « Mechanical Properties and Mullins Effect in Natural Rubber Reinforced by Grafted Carbon Black », *Advances in Polymer Technology*, 2019. https://www.hindawi.com/journals/apt/2019/4523696/abs/ (consulté le août 10, 2019).

[37] R. Dargazany et M. Itskov, « Constitutive modeling of the Mullins effect and cyclic stress softening in filled elastomers », *Phys. Rev. E*, vol. 88, n° 1, p. 012602, 2013, doi: 10.1103/PhysRevE.88.012602.

[38] E. Guth, « Theory of Filler Reinforcement », *J. Appl. Phys.*, vol. 16, n° 1, p. 20‑25, 1945, doi: 10.1063/1.1707495.

[39] A. I. Medalia, « Morphology of aggregates: VI. Effective volume of aggregates of carbon black from electron microscopy; Application to vehicle absorption and to die swell of filled rubber », *J. Colloid Interface Sci.*, vol. 32, n° 1, p. 115‑131, 1970, doi: 10.1016/0021-9797(70)90108-6.

[40] M. R. Kashani et J. Padovan, « Modelling reinforcement of rubber with carbon black filler », *Plast. Rubber Compos.*, vol. 36, n° 2, p. 47‑55, 2007, doi: 10.1179/174328907X171208.

[41] B. Omnès, S. Thuillier, P. Pilvin, Y. Grohens, et S. Gillet, « Effective properties of carbon black filled natural rubber: Experiments and modeling », *Compos. Part Appl. Sci. Manuf.*, vol. 39, n° 7, p. 1141‑1149, 2008, doi: 10.1016/j.compositesa.2008.04.003.

[42] N. Candau, « Compréhension des mécanismes de cristallisation sous tension des élastomères en conditions quasi-statiques et dynamiques », thesis, INSA Lyon, 2014.

[43] V. Litvinov, R. A. Orza, M. Klueppel, M. Duin, et P. Magusin, « Rubber–Filler Interactions and Network Structure in Relation to Stress–Strain Behavior of Vulcanized, Carbon Black Filled EPDM », *Macromolecules*, vol. 44, p. 4887–4900, juin 2011, doi: 10.1021/ma2007255.

[44] D. Richter, B. Farago, R. Butera, L. J. Fetters, J. S. Huang, et B. Ewen, « On the origins of entanglement constraints », *Macromolecules*, vol. 26, n° 4, p. 795‑804, 1993, doi: 10.1021/ma00056a034.

[45] G. Chagnon, E. Verron, G. Marckmann, et L. Gornet, « Development of new constitutive equations for the Mullins effect in rubber using the network alteration theory », *Int. J. Solids Struct.*, vol. 43, n° 22, p. 6817‑6831, 2006, doi: 10.1016/j.ijsolstr.2006.02.011.

[46] J. Diani, M. Brieu, et J. M. Vacherand, « A damage directional constitutive model for Mullins effect with permanent set and induced anisotropy », *Eur. J. Mech. - ASolids*, vol. 25, n° 3, p. 483‑496, 2006, doi: 10.1016/j.euromechsol.2005.09.011.

[47] G. Marckmann, E. Verron, L. Gornet, G. Chagnon, P. Charrier, et P. Fort, « A theory of network alteration for the Mullins effect », *J. Mech. Phys. Solids*, vol. 50, n° 9, p. 2011‑2028, 2002, doi: 10.1016/S0022-5096(01)00136-3.

[48] A. N. Gent, *Engineering with Rubber: How to Design Rubber Components*, 3e éd. München: Carl Hanser Verlag GmbH & Co. KG, 2012.

[49] G. Machado, G. Chagnon, et D. Favier, « Induced anisotropy by the Mullins effect in filled silicone rubber », *Mech. Mater.*, vol. 50, p. 70‑80, 2012, doi: 10.1016/j.mechmat.2012.03.006.

[50] K. Yamaguchi, J. J. C. Busfield, et A. G. Thomas, « Electrical and mechanical behavior of filled elastomers. I. The effect of strain », *J. Polym. Sci. Part B Polym. Phys.*, vol. 41, n° 17, p. 2079‑2089, 2003, doi: 10.1002/polb.10571.

[51] A. K. M. Idrissa, S. Ahzi, S. Patlazhan, Y. Rémond, et D. Ruch, « A constitutive model for stress–strain response and mullins effect in filled elastomers », *J. Appl. Polym. Sci.*, vol. 125, n° 6, p. 4368‑4375, 2012, doi: 10.1002/app.36596.

[52] Y. Fukahori, « New progress in the theory and model of carbon black reinforcement of elastomers », *J. Appl. Polym. Sci.*, vol. 95, n° 1, p. 60‑67, 2005, doi: 10.1002/app.20802.

[53] O. Oguz, N. Candau, M. K. Citak, F. N. Cetin, S. Avaz Seven, et Y. Z. Menceloglu, « A Sustainable Approach to Produce Stiff, Super-Tough, and Heat-Resistant Poly(lactic acid)-Based Green Materials », *ACS Sustain. Chem. Eng.*, vol. 7, n° 8, p. 7869‑7877, 2019, doi: 10.1021/acssuschemeng.9b00319.

[54] O. Oguz *et al.*, « High-Performance Green Composites of Poly(lactic acid) and Waste Cellulose Fibers Prepared by High-Shear Thermokinetic Mixing », *Ind. Eng. Chem. Res.*, vol. 56, n° 30, p. 8568‑8579, 2017, doi: 10.1021/acs.iecr.7b02037.